

REPORT DOCUMENTATION PAGE

Form Approved
OMB No. 0704-0188

Public reporting burden for this collection of information is estimated to average 1 hour per response, including the time for reviewing instructions, searching existing data sources, gathering and maintaining the data needed, and completing and reviewing this collection of information. Send comments regarding this burden estimate or any other aspect of this collection of information, including suggestions for reducing this burden to Department of Defense, Washington Headquarters Services, Directorate for Information Operations and Reports (0704-0188), 1215 Jefferson Davis Highway, Suite 1204, Arlington, VA 22202-4302. Respondents should be aware that notwithstanding any other provision of law, no person shall be subject to any penalty for failing to comply with a collection of information if it does not display a currently valid OMB control number. **PLEASE DO NOT RETURN YOUR FORM TO THE ABOVE ADDRESS.**

| | | | | | |
|--|--------------------|-----------------------|---|----------------------------|--|
| 1. REPORT DATE (DD-MM-YYYY) | | 2. REPORT TYPE | 3. DATES COVERED (From - To) | | |
| 4. TITLE AND SUBTITLE | | | 5a. CONTRACT NUMBER | | |
| | | | 5b. GRANT NUMBER | | |
| | | | 5c. PROGRAM ELEMENT NUMBER | | |
| 6. AUTHOR(S) | | | 5d. PROJECT NUMBER | | |
| | | | 5e. TASK NUMBER | | |
| | | | 5f. WORK UNIT NUMBER | | |
| 7. PERFORMING ORGANIZATION NAME(S) AND ADDRESS(ES) | | | 8. PERFORMING ORGANIZATION REPORT NUMBER | | |
| 9. SPONSORING / MONITORING AGENCY NAME(S) AND ADDRESS(ES) | | | 10. SPONSOR/MONITOR'S ACRONYM(S) | | |
| | | | 11. SPONSOR/MONITOR'S REPORT NUMBER(S) | | |
| 12. DISTRIBUTION / AVAILABILITY STATEMENT | | | | | |
| 13. SUPPLEMENTARY NOTES | | | | | |
| 14. ABSTRACT | | | | | |
| 15. SUBJECT TERMS | | | | | |
| 16. SECURITY CLASSIFICATION OF: | | | 17. LIMITATION OF ABSTRACT | 18. NUMBER OF PAGES | 19a. NAME OF RESPONSIBLE PERSON |
| a. REPORT | b. ABSTRACT | c. THIS PAGE | | | 19b. TELEPHONE NUMBER (include area code) |

**Design, Fabrication and Testing of a
Passively Morphing Ornithopter Wing for Increased Lift and Agility**

AFOSR Final Technical Report

FA9550-09-1-0632

Program Manager: Dr. David Stargel

Principal Investigators: Dr. James E. Hubbard Jr. and Dr. Mary I. Frecker

Submitted on: 12/13/2012

Abstract

Over the last few decades, flapping wing Unmanned Aerial Vehicles (UAVs), or ornithopters, have shown the potential for advancing and revolutionizing platform performance in both the civil and military sectors. An ornithopter is unique in that it can combine the agility and maneuverability of rotary wing aircraft with excellent performance in low Reynolds number flight regimes. The objective of the proposed work was to develop methods to design novel ornithopter wings that allow passive wing morphing. Passive morphing was achieved through an optimally designed compliant spine that mimics the function of a bird's wrist. A multi-objective optimization was carried out and several designs resulting from this optimization were bench-top and free flight tested. The presence of a 1DOF compliant spine in the ornithopter wing was found to introduce an asymmetry between the upstroke and the downstroke. For any given flapping frequency or throttle setting, the ornithopter with the compliant spine consumed less electric power, produced more mean lift and did not incur any thrust penalties when compared to the ornithopter without the compliant spine. Power reduction of 44.7% was achieved at the steady level flight flapping frequency, lift gains of up to 16% of the ornithopter's weight was also realized without incurring any thrust penalties. Also during the free flight test, the ornithopter with the compliant spine inserted in its wings reduced the overall negative center of mass acceleration during one flapping cycle by 22 %. The negative acceleration reduction may translate into overall lift gains. Thus the steady level flight performance was improved due to the presence of the compliant spine. Therefore compliant mechanisms proved to be not only feasible, but also beneficial for application to general air vehicle design.

1. Introduction

1.1. Objective

The objective of the proposed work was to develop methods to design novel ornithopter wings that allow passive wing morphing. Passive morphing is achieved through an optimally designed compliant spine that mimics the function of a bird's wrist. This work enables the design of flapping wing vehicles which can be tailored to provide improved lift for takeoff or increased thrust for forward, straight and level flight as compared to conventional non-morphing wings. Furthermore these passively morphing wings make no additional power demands that require specialized motors or servos. They are designed to mitigate the detrimental impact of increased drag on the upstroke by allowing the outmost section of the wing to deflect downward, while maintaining the thrust performance of a rigid wing during the downstroke cycle. Our passive morphing wing design results have demonstrated a range of motion and wing shape not possible with rigid wings.

1.2. Program Significance

Over the last few decades, flapping wing Unmanned Aerial Vehicles (UAVs), or ornithopters, have shown the potential for advancing and revolutionizing platform performance in both the civil and military sectors[1]. An ornithopter is unique in that it can combine the agility and maneuverability of rotary wing aircraft with excellent performance in low Reynolds number flight regimes. These traits yield optimized performance over multiple mission scenarios. Nature achieves such performance in birds using wing gaits or kinematics that are optimized for various flight conditions, as shown in Figure 1.1[2,3].



Figure 1.1: Wing configurations used for a particular flight condition.

Current state of the art designs for wing morphing utilize rigid-link mechanisms such as four-bar mechanisms or they involve active morphing techniques[4-6]. In contrast to rigid-link mechanisms and active approaches, the focus of this work was on the implementation of a novel *passive* morphing technique using nonlinear compliant mechanisms. When compared to active morphing, passive morphing mechanisms require no additional energy expenditure, minimal weight addition and low complexity. Moreover, there is no phase lead/lag between the flapping and the morphing mechanisms, as the morphing is due to only the aerodynamic loads experienced by the ornithopter during flight.

1.3. Air Force Relevance

The Air Force has expressed an interest in improving the aerodynamic performance of vehicles using compliant mechanisms. In a recent workshop hosted by AFRL/AFOSR in March 2012, researchers in compliant mechanism design, adaptive structures, and aircraft structural design came together to share their current work and to develop collaborations. The aim was to investigate the feasibility of applying compliant mechanism design methodology to general air vehicle design and to develop synergies leading to more affordable and reliable air vehicle designs. The PI's have been working toward achieving this vision since 2009, as evidenced by the successful development and implementation of a passive compliant spine for ornithopter application[7]. During the performance period of the grant summarized in this report, compliant mechanisms were successfully integrated into test ornithopters to maximize energy efficiency and geometric advantages. The research approach was unique in that it exploited the normal operational loads experienced by the flight platform in order to achieve the desired wing deflections, thus improving performance without relying on complex actuators and mechanisms. The work reported herein has introduced and validated a novel technique of using compliant mechanisms to passively achieve morphing on lifting and thrusting surfaces. This technique can be applied to air vehicles of various scales, from insect and avian-scale to full-scale. This research is important to the Air Force's efforts in extending the application of compliant mechanisms to aeronautics and aerospace systems to solve immediate and future challenges.

1.4. Accomplishments

The key accomplishments and contributions of the work supported by grant FA9550-09-1-0632 are as follows:

- Developed compliant spine architecture for passive wing morphing.
- Quantified avian wing gaits to use as inputs to the compliant spine design optimization.
- Developed design optimization algorithms for compliant spine.
- Fabricated and integrated compliant spine into test ornithopters.
- Measured the performance of test ornithopters with and without compliant spines in order to quantify the effect on steady level flight performance during bench testing.

- Developed a novel free flight testing technique for flapping wing vehicles
- Completed extensive free flight testing at Wright Patterson Air Force Base Micro Air Vehicle Indoor Flight lab that set several precedents where optimized compliant spines were inserted in the ornithopter's leading edge spar. Precedents set include largest flapping wing vehicle to fly in the facility with the most number of reflective markers.
- Measured the performance of test ornithopters with and without compliant spines in order to quantify the effect on steady level flight performance during free flight testing.
- Bench and flight test showed that the ornithopter with the compliant spine consumed less electric power, produced more mean lift and did not incur any thrust penalties when compared to the ornithopter without the compliant spine.

2. Bio-Inspired Design: Background

The benefits and efficacy of passive wing morphing attained by introducing an asymmetry in the leading edge wing spar kinematics during the up and down strokes has been investigated[8,9]. Billingsely et al. installed passive torsional springs in the leading edge spar at the wing half span to exploit the advantages of wing surface area reduction during the upstroke[9]. These springs were designed to deflect on the upstroke only and lock during the downstroke. Wing bending during the upstroke reduces the wing relative area (i.e., the wing area perpendicular to the flapping motion), which in turn mitigates the drag penalties experienced by the test ornithopter during this portion of its wing beat cycle.

While the results of Billingsely's experiment showed a 300% increase in net lift, there were also significant thrust penalties. It was concluded that more sophisticated wing kinematics are required in order to maintain the lift gains while mitigating thrust penalties thus improving the overall aerodynamic performance of the ornithopter. The desired kinematics can be observed in natural avian flyers. An example is the avian gait known as the Continuous Vortex Gait (CVG) is shown in Figure 3.1 [10]. A detailed discussion of the kinematics of the CVG can be found in [2] and[3]. The advantage of using the CVG is that it is an avian gait that can be implemented passively because it requires motion in only one major joint, namely the wrist. In order to implement the CVG on a test ornithopter and achieve improved performance, specific wing kinematics are required. The outer section of the wing has to bend, sweep and twist simultaneously during the upstroke, while remaining fully extended during the downstroke. To attain the desired kinematics, a novel compliant spine was designed, fabricated and integrated into the leading edge wing spar at 37% of the wing half span of a test ornithopter in order to mimic the function of an avian wrist. The motion described above (bending, sweep and twist) requires a 3 degree of freedom spine. As a first step to achieving this gait, single degree of freedom (1 DOF) spines were designed, fabricated, and tested.

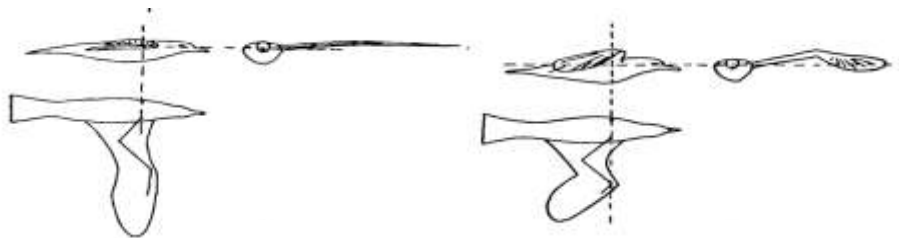


Figure 3.1. During the continuous vortex gait the wings are fully extended at mid downstroke (left) and bent, twisted and swept at mid upstroke (right) [10].

The remainder of this report is organized as follows: The design optimization of the 1DOF compliant spines is described in Section 3. Several prototypes were evaluated experimentally; the experimental

procedures used to test the compliant spines is described in Section 4. The results of the experimental evaluation of the ornithopter with and without the compliant spines is presented in Section 5.

3. Design Optimization

A Compliant Spine (CS) is a contact-aided compliant mechanism with tailorable nonlinear stiffness properties. This mechanism, when inserted in the leading edge spar, allows the wingtips to undergo the desired deflections during upstroke, while remaining stiff during the downstroke. Figure 3.1 shows a CS design with three compliant joints (CJs). Note that this design is flexible in bending in the upstroke direction because of the deflection of semi-circular compliant hinges (CHs), and it is very stiff in bending during downstroke because the slanted faces come into contact with one another.

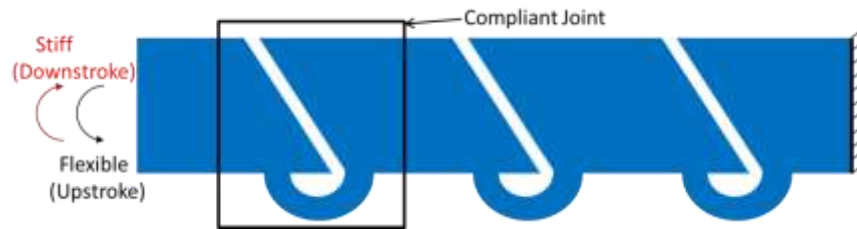


Figure 3.1 A CS design with three CJs.

An optimal CS is necessary for ornithopter applications to achieve the desired kinematics of the wing without adding excessive weight or generating excessive stresses. The parameters that affect the performance of a compliant spine are the number of compliant joints and the design of each CJ. A single CJ of a CS is shown in Figure 3.2, where the inner and outer surfaces of the compliant hinge were assumed to be semicircles. This assumption was based on a previous optimization study performed on a single compliant hinge[11]. Design parameters that affect the design of the compliant joint were the contact angle (ϕ), contact gap (g_c), inner radius of the compliant hinge (R_{in}), outer radius of the compliant hinge (R_{out}), and eccentricity of the compliant hinge (e), as shown in Figure 3.2. The black dot in the figure represents the center of the outer semi-circle and the red star represents the center of the inner semi-circle of the compliant hinge. The value of the eccentricity e is positive if the black dot is to the right of the red star and is negative if it is otherwise, except when the black dot and red star coincide, then e has a value of zero. The contact gap (g_c) of a compliant joint is the perpendicular distance between the slanted contact surfaces.

The effects of the contact gap and contact angle on the downstroke performance of a single compliant joint were studied and presented in [11]. It was found that for optimal performance of a CJ, the contact angle (ϕ) must be 130° and that the contact gap in a CJ must be as small as possible for minimum downstroke deflection of the CS. The minimum contact gap size is based on the manufacturing process used to fabricate the CS.

With the contact angle and gap fixed, three parameters remain as variables, the inner and outer radii of the compliant hinge and the eccentricity of the compliant hinge. These three design parameters will dictate the geometry of a single compliant joint, and therefore the optimization was applied to these three variables that affect the upstroke deflection. In addition to the compliant hinge geometry, the number of compliant joints also affects the upstroke performance of a CS. The optimization problem, formulated below, was solved for a fixed number of compliant joints, selected by the designer. The number of design variables in the optimization problem was then three times the number of compliant joints.

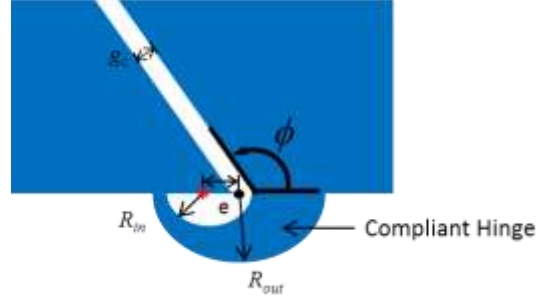


Figure 3.2 A CS with single CJ and its design parameters.

The multi objective optimization problem formulated to design an optimal compliant spine is shown in Equations 1-9:

$$\begin{aligned} & \text{Minimize } (f_1, f_3) \\ & \text{Maximize } (f_2) \end{aligned}$$

S.T.

$$\left. \begin{aligned} R_{kin} - R_{kout} &\leq 0 \\ R_{kin} - R_{kout} + |e_k| &\leq 0 \\ lb_{in} &\leq R_{kin} \leq ub_{in} \\ lb_{out} &\leq R_{kout} \leq ub_{out} \\ lb_e &\leq e_k \leq ub_e \end{aligned} \right\} \mathbf{k} = 1, 2, 3, \dots, T \quad (1)$$

Where,

$$f_1 = \lambda * M + (1 - \lambda) * M_{penalty} \quad (2)$$

$$f_2 = \lambda * Z_{max} - (1 - \lambda) * Z_{penalty} \quad (3)$$

$$f_3 = \lambda * \sigma_{max} + (1 - \lambda) * \sigma_{penalty} \quad (4)$$

$$\lambda = \begin{cases} 1 & \text{if } \sigma_{max} \leq \sigma_{cutoff} \\ 0 & \text{if } \sigma_{max} > \sigma_{cutoff} \end{cases} \quad (5)$$

$$\sigma_{cutoff} = \alpha * \sigma_{yield} \quad (6)$$

$$M_{penalty} \gg M \quad (7)$$

$$Z_{penalty} \ll Z_{max} \quad (8)$$

$$\sigma_{penalty} \gg \sigma_{max} \quad (9)$$

Geometric constraints on the design variables, given by Equation 1, ensure that the inner and outer semi-circles of the hinges never intersect, thus creating feasible compliant hinges for all the CS designs. The objective functions f_1 , f_2 , and f_3 , are measures of the mass, tip deflection and peak stress in the compliant spine, respectively, and are given by Equations 2, 3, and 4. They were calculated using a commercial finite element package, ANSYS. A controlled elitist genetic algorithm, which is a variant of NSGA-II [12,13] was used to solve this multi-objective optimization problem. This genetic algorithm (GA) was part of the optimization toolbox provided in MATLAB.

Constraints on the objective functions are imposed using penalty the values $M_{penalty}$, $Z_{penalty}$, and $\sigma_{penalty}$ and the binary variable λ . These penalty values (Equations 7, 8, and 9) were chosen such that an infeasible design, determined by Equation 5, was assigned a poor value of the objective function; such designs are terminated and not allowed to propagate into future generations. Computational time was also an important factor in this optimization because dynamic analysis was being performed on each of the CS

designs in each generation. Taking the computational resources and complexity of the problem into consideration, penalty values proved to be very effective in driving the optimization towards feasible regions in the design space. A CS design was considered to be infeasible if the maximum von Mises stress in the design, after dynamic analysis, was greater than a cutoff stress limit, calculated from Equation 6. This limit was controlled by the designer by choosing an appropriate value for α , which can be a function of the safety factor. The optimization problem was then implemented using the algorithm shown in the schematic in Figure 3.3.

This design optimization procedure along with a quantitative convergence metric was implemented for CSs with two, three and four compliant joints. Those optimization results are shown Figure 3.4. Pareto fronts of two, three and four Compliant Joint Compliant Spines (CJCSs) were shown in Figure 3.4 (a), (b), and (c). It can be seen from the figures that the Pareto fronts are not convex and there are certain trends in the objective functions as the number of compliant joints increase. Figure 3.4 (a) shows that for a particular stress, the deflection of a four CJCS is almost always more than the deflection of a two CJCS, and the Pareto front of a three CJCS lies in between the Pareto fronts of four CJCS and two CJCS. It can also be observed that the lower left corner of figure 3.4(a) is dominated by the two CJCS designs (blue points). This suggests that, for a particular loading condition, the stiffness of a design is a function of the number of joints and the minimum possible deflection is higher for a design with more number of joints. Figure 3.4(b) suggests that for a particular stress, the four CJCS designs are always more massive than two or three CJCS designs. Figure 3.4(c) suggests that four CJCSs have greater mass than the two CJCSs and the three CJCSs, but they also have greater maximum possible deflection values. Thus from Figures 3.4(b) and (c), it is evident that a compliant joint adds a small amount of mass to the CS but decreases its stiffness at the same time. Therefore there is a tradeoff between the number of compliant joints (or mass) and the desired deflection. Three optimal compliant spines obtained from this optimization were chosen for flight-testing purposes. They are shown in Figure 3.4(d).

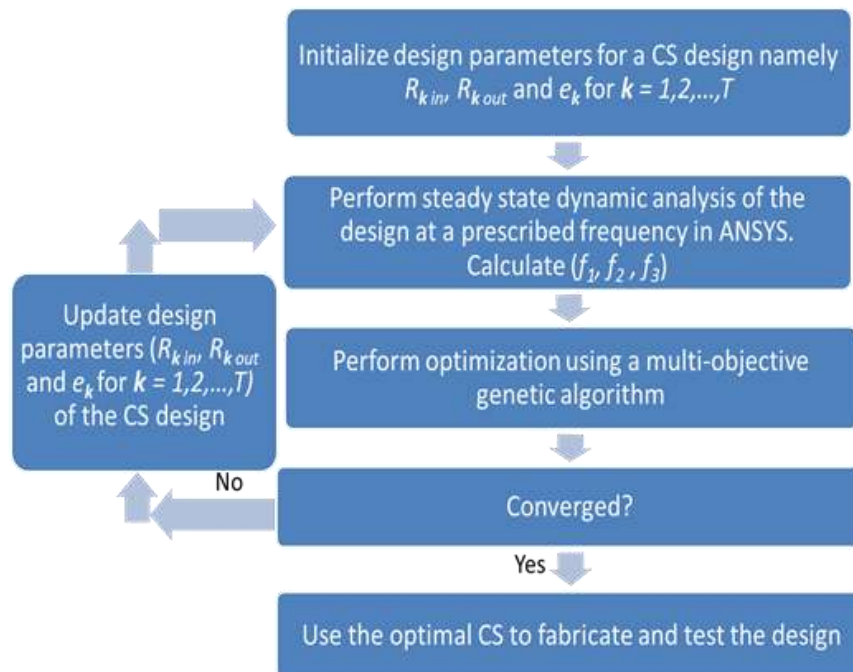


Figure 3.3 Schematic representation of optimization procedure

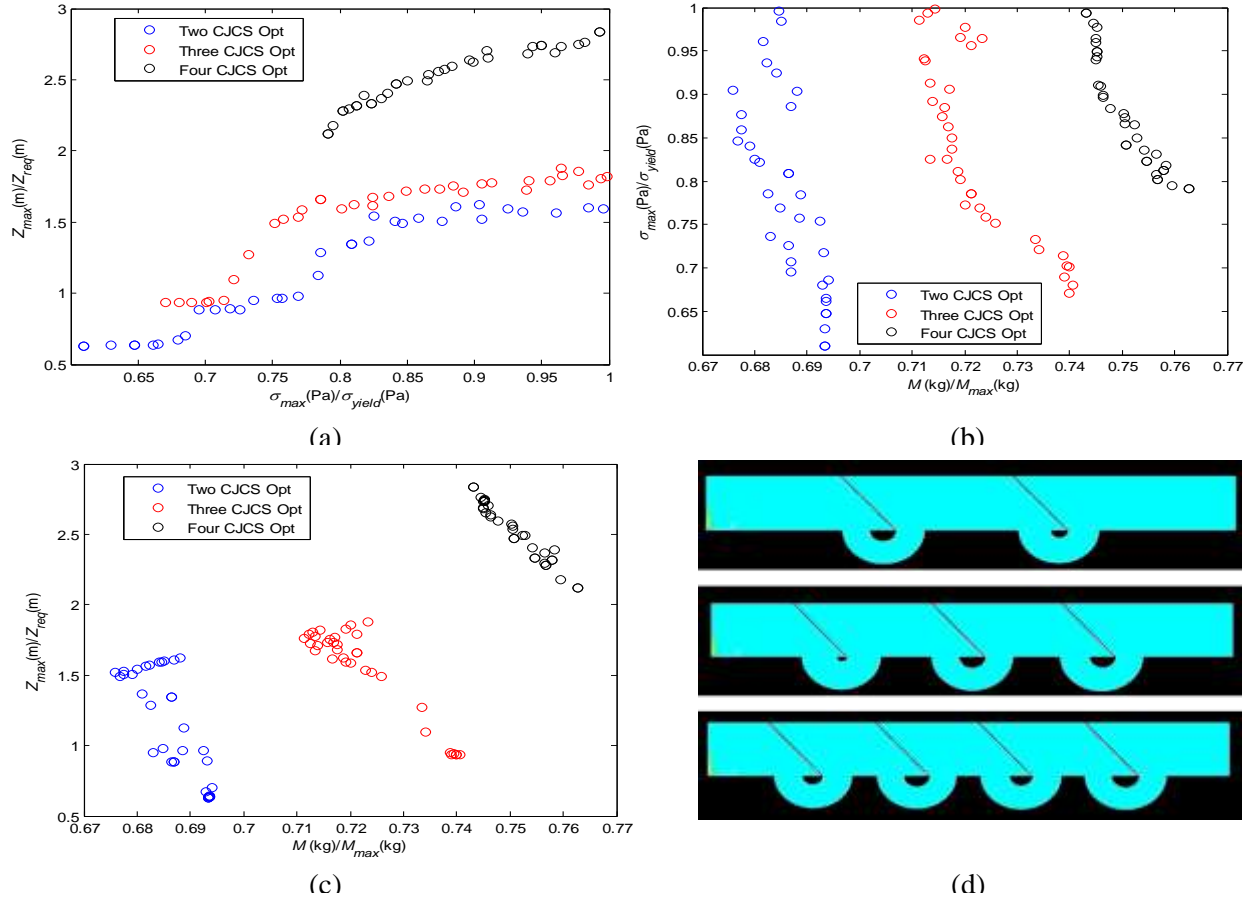


Figure 3.4. Multi-objective CS dynamic optimization results (a) Pareto plot comparing deflection and stress (b) Pareto plot comparing maximum stress and mass of the compliant spines (c) Pareto plot comparing deflection and mass of the compliant spines (d) Optimal compliant spines that were used for successful flight testing.

Implementing CVG in an ornithopter requires bending, sweeping, and twisting of the wings. A CS is a 1 DOF mechanism and causes bending alone of the wings. To achieve all three simultaneously, two more contact aided compliant mechanisms called compliant elements were designed. They are bend-and-sweep compliant element (Figure 3.5(a)) and twist compliant element (Figure 3.5(b)). These compliant elements have unique, nonlinear stiffness properties and utilize self-contact. Bend-and-sweep compliant element can be used to achieve passive bending and sweeping of ornithopter’s wings simultaneously. Twist compliant element can be used to achieve twist alone.

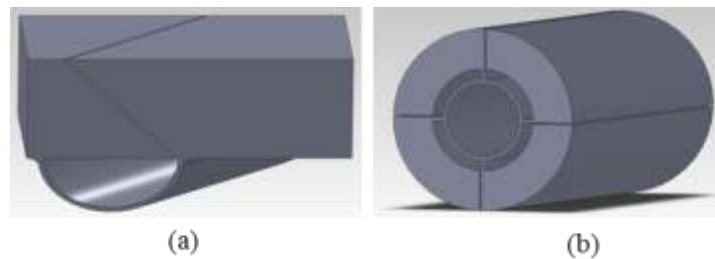


Figure 3.5. Contact aided compliant mechanisms with tailorable nonlinear stiffness. (a) Bend-and-Sweep Compliant Element (b) Twist Compliant Element.

4. Experimental Set up and Procedures

4.1. Bench Test

Based on preliminary quasi-static analyses and optimization, an acceptable compliant spine design was selected for prototyping and testing. The compliant spine consisted of three compliant hinges, with each compliant hinge consisting of two concentric semicircles. This compliant spine was made of Delrin and was attached to the spar with the help of 10-32 nylon bolts as shown in Figure 4.1. The test ornithopter used was a commercially available Park Hawk Model, which had a wing span of 1.07m (42"). The ornithopter's mass without any payload was 425 g.

The ornithopter wing flapping rate was between 4 and 6 Hz, with a forward speed range of 10 - 30 km/h, and a distance range of 0.8 km [14]. The performance of the test ornithopter was measured with and without the compliant spine inserted into the leading edge spars. Three performance metrics were selected as a basis of comparison for the test ornithopter.

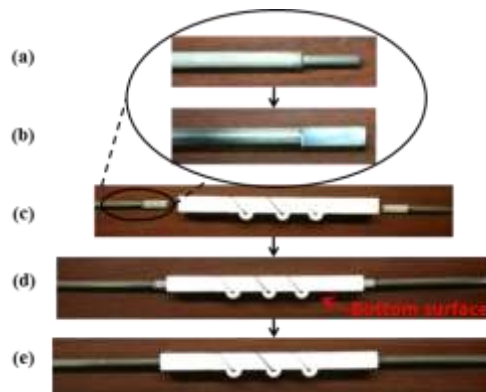


Figure 4.1. The compliant spine was attached to the spar (a) with the help of 10-32 Nylon bolts. The bolts were glued to both ends of the spar as shown in (b) and (c). Then the spars were screwed into the ends of the spine as shown in (d) and (e).

The first performance metric was the electric power used by the flapping mechanism. In order to calculate the electric power, both the current and the voltage drawn from the power supply during flapping were measured. Once the current and the voltage were measured, the electric power consumed by the ornithopter at various flapping frequencies was calculated. The second set of performance metrics were the lift and thrust produced by the ornithopter. A six degree of freedom strain gauge transducer manufactured by Advanced Mechanical Technology Inc. was used to measure the lift and thrust produced by the test ornithopter at various flapping frequencies, with and without the compliant spine inserted in the leading edge spars. Figure 4.2 (a) and Figure 4.2 (b) show the test ornithopter mounted on a 6 degree of freedom load cell. The third set of performance metrics were the wing tip and spine tip bending deflections. To capture the bending deflections of the wing during the up and down strokes, three red markers were placed on the leading edge spar. One marker was placed at the wing root, another was placed at the location of the compliant spine tip and a third marker was placed at the wing tip.



Figure 4.2.(a) Test ornithopter mounted on a six channel load cell to measure the lift and thrust produced at various flapping frequencies. (b) The compliant spine was inserted at the leading edge spar of the test ornithopter at 37% of the wing half span to mimic the function of an avian wrist.

4.2. Free Flight Test

Free flight tests were conducted at Wright Patterson Air Force Base (WPAFB) in the Air Force Research Lab's (AFRL) Indoor Micro Air Vehicle (MAV) laboratory with the help of Dr. Richard Roberts, Dr. Gregory Park, and Dr. Gregory Reich. The AFRL MAV indoor flight test laboratory is the largest Vicon motion capture system lab in the United States. The laboratory is composed of a large test chamber and a co-located control room. The test chamber is roughly 55' x 70' x 35'. Instrumentation consists of a VICON motion capture system with 60 motion capture cameras. By adding small retro-reflective markers to a vehicle, the VICON system can track position and orientation of the vehicle with an accuracy of ~1.0 mm. For the aforementioned flight test, fifty-three 6.34 mm diameter reflective ball markers were bonded to the test vehicle in locations that were deemed necessary in order to obtain sufficient data to fully characterize the wings. The Vicon® motion capturing system was used to capture and contrast the wing 3D kinematics of the ornithopter with and without the compliant spine inserted in the leading edge spar. Figure 4.3 shows a picture of the test platform in the flight lab and the placement of the reflective markers, respectively.



Figure 4.3. (a) Test platform in the AFRL MAV flight lab. (b) Reflective Markers Placement: 47 markers were placed on the wings and tail, 5 markers were placed on the fuselage and 1 marker was placed on the ornithopter's shoulder joint.

The University of Maryland Morpheus laboratory has developed a novel technique that permits the free flight testing of an avian scale flapping wing vehicle. For the test set-up an eighty pound fishing line was strung between two trusses at opposite corners of the flight lab at approximately 7 foot height. The vehicle was hung from a lead wire off this tether in order to constrain the vehicle flight path, as well as to

prevent impacts. The lead line was able to slide on the tether by using a fishing barrel swivel. Figure 4.4(a) shows a schematic of the test set-up.

Using the aforementioned test set-up, five ornithopter wing configurations were tested. The first configuration was a solid ornithopter wing spar, consisting of a uniform rigid carbon fiber leading edge spar. The rest of the configurations tested were a compliant ornithopter wing spar, which contained a compliant mechanism inserted in its leading edge spar. The four compliant spines configurations that were tested are shown in Figure 3.4(d) along with the compliant spine that was previously tested during the bench test. All of the compliant spines were 2.5" in length with 1" tab on both sides to allow for attachment to the leading edge spar. The test compliant spine was attached to the carbon fiber spar using six 5-40 bolts and a Delrin collar, as shown in Figure 4.4 (b). The major differences between the various compliant spine designs were the number of compliant hinges and the loading condition applied during their design optimization process.

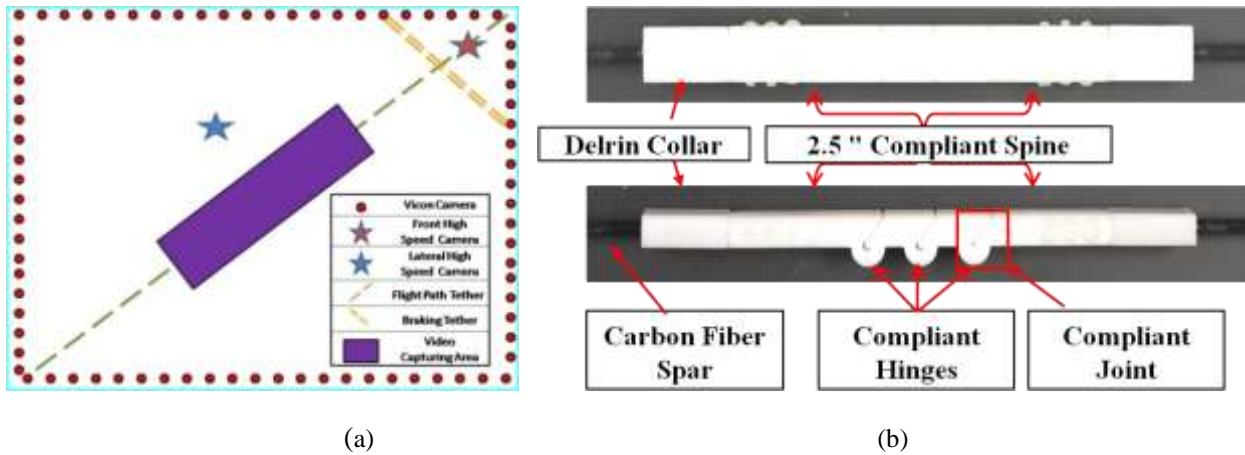


Figure 4.4. (a) Test Setup Schematic. (b) Compliant Spine Assembly Components

5. Experimental Results

5.1. Bench Test Results

Bench test data were collected at various flapping frequencies, where the flapping frequency was controlled by the throttle position on a remote control radio transmitter. The “solid” data corresponds to the performance of the ornithopter with the solid leading edge spar without the compliant spine insert, and the “compliant” data corresponds to the performance of the ornithopter with the compliant spine inserted in the wings leading edge spar. A detailed discussion of the bench test results has been presented in [7,15]. Figures 5.1 (a) and (b) show the electric power consumed by the ornithopter at various flapping frequencies, and the flapping frequency versus the percentage throttle, respectively. Also Figures 5.2 (a) and (b) show the mean lift and mean thrust produced by the ornithopter versus the percentage throttle.

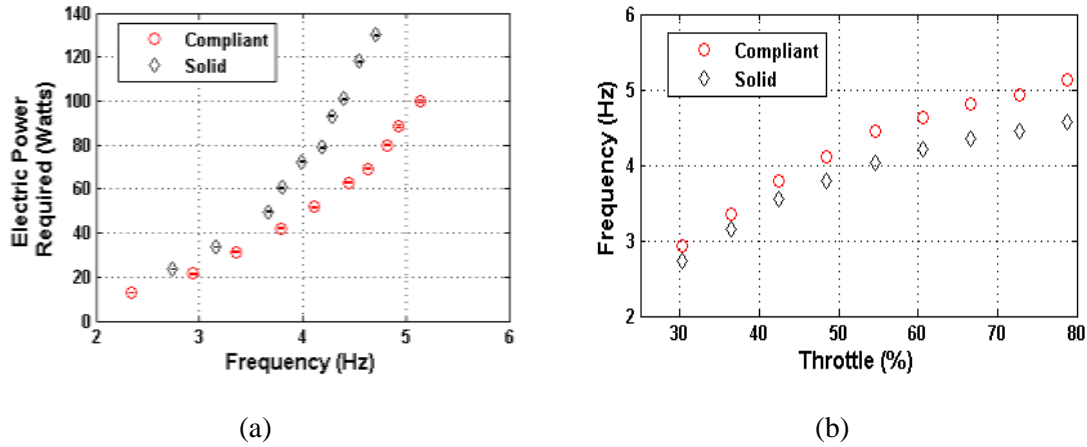


Figure 5.1.(a) The electric power required vs. flapping frequency. (b) Flapping frequency vs. percentage throttle.

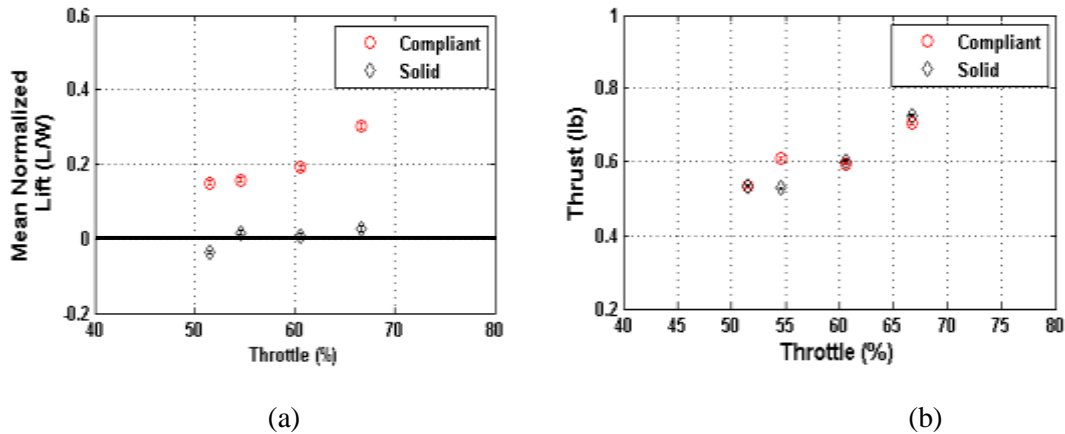


Figure 5.2. (a) Mean normalized lift versus throttle position plot. (b) Mean thrust versus throttle position plot

From Figure 5.1(a), it can be observed that the test ornithopter with the compliant spine insert consumes less power than it does without the compliant spine, for all flapping frequencies. At a flapping frequency of 4.7 Hz the power savings due to the presence of the compliant spine was 44.7%. Also Figure 5.1(b) shows that the ornithopter with the compliant spine inserted in its wings operated at a higher flapping frequency for all throttle inputs. As for the aerodynamic loads produced by the ornithopter, Figure 5.2 (a) shows that by inserting the compliant spine into the spars, an asymmetry is introduced between the up and down strokes which caused an increase in the mean lift. Moreover at the steady level flight flapping frequency of 4.7 Hz, the ornithopter with the compliant spine produced mean lift supporting 16% of its body weight. This lift gain could not be produced under the same conditions with a solid leading edge wing spar. This increase in mean lift can be directly translated into improved payload capability. Figure 5.2 (b) shows that for any given throttle input, the mean thrust produced by the ornithopter with and without the compliant spine are similar, hence it is concluded that the compliant spine was successful at producing lift gains without incurring any significant thrust penalties.

Lastly the wing kinematics of the solid and compliant spars captured using high speed photography were compared. The compliant spine was designed to bend during the upstroke while remaining stiff (i.e.,

mimicking a solid spar) during the downstroke. Figure 5.3 compares the bending deflections of the wing with the compliant and solid spars at mid downstroke and mid upstroke.

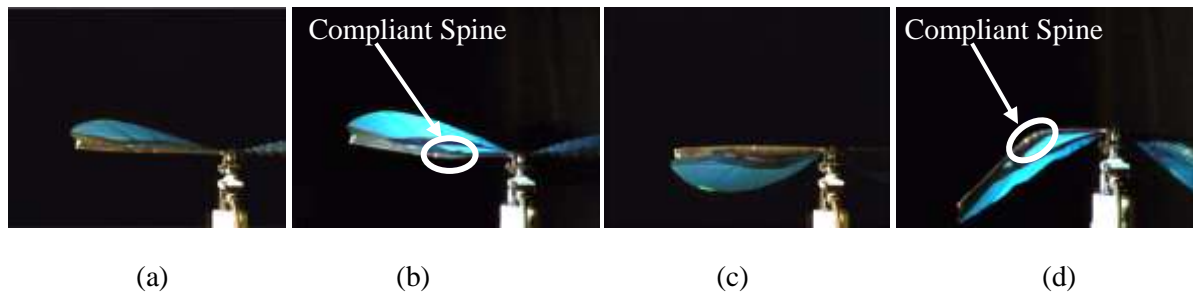


Figure 5.3. (a) Wing bending deflections at mid downstroke for the ornithopter with the solid spar, i.e., without the compliant spine. (b) Wing bending deflections at mid downstroke for the ornithopter with the compliant spine. (c) Wing bending deflections at mid upstroke for the ornithopter with the solid spar, i.e., without the compliant spine. (d) Wing bending deflections at mid upstroke for the ornithopter with the compliant spine.

Both Figures 5.3(a) and (b) show comparable deformation during the downstroke indicating that the compliant spine mimics the solid spar, while Figures 5.3(c) and 5.3(d) shows that the wing with the compliant spine had a greater deflection than that without the compliant spine during the upstroke. Table 1 shows the bending deflections at the location of the compliant spine tip relative to the wing root for the wing with and without the compliant spine at a flapping frequency of 4.7 Hz. These deflections were calculated by determining the difference between the vertical location of the middle bending deflection marker and the root bending deflection marker, mentioned in Section 4.1, for the wing with and without the compliant spine.

Table 1. Bending deflections at the location of the compliant spine tip relative to the wing root*.

| Wing Position | With Compliant Spine (cm) | Without Compliant Spine (cm) | Difference in Deflections (cm) |
|----------------|---------------------------|------------------------------|--------------------------------|
| Mid Downstroke | -3.41 | -2.57 | -0.84 |
| Mid Upstroke | 4.07 | 0.72 | 3.36 |

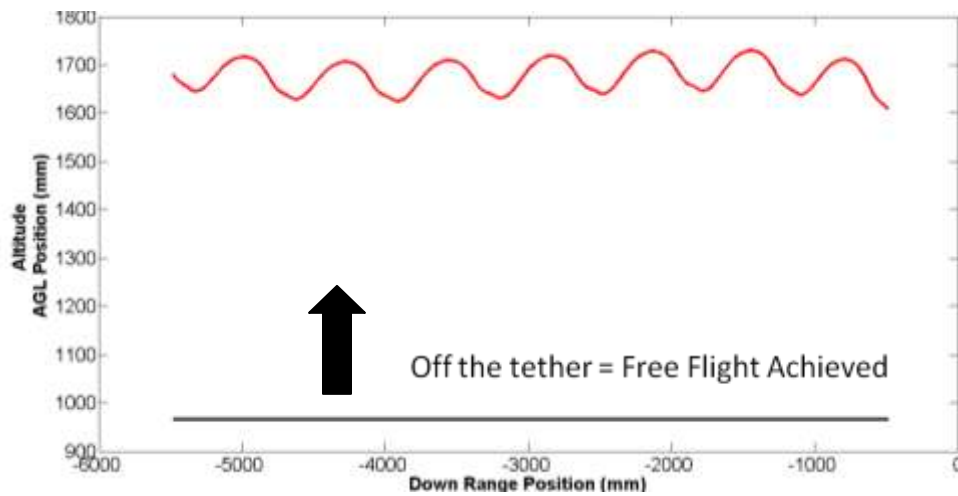
* Negative bending is upwards bending, positive bending is downwards bending.

The data in Table 1 along with Figure 5.3 show that during the downstroke the bending deflection of the wings with and without the compliant spine were similar. Meanwhile during the upstroke, the bending deflection of the wing with the compliant spine is larger than the wing without the compliant spine. The bending deflections due the presence of the compliant spine during the upstroke leads to a reduction of the wing relative surface area and therefore a decrease in the amount of negative lift and drag produced during that portion during this portion of the wing beat cycle.

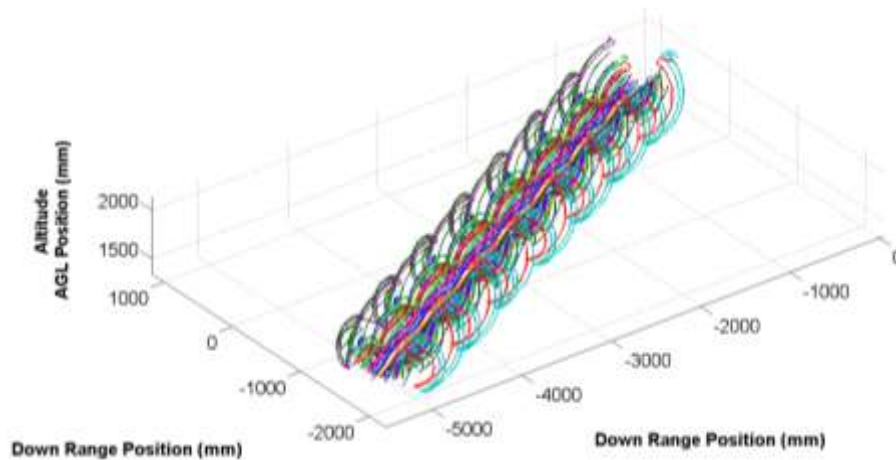
5.2. Free Flight Testing

A primary goal of the flight test was to compare the kinematics of the ornithopter with and without the compliant spine inserted in its wings, and then ultimately use these kinematics to investigate the effect of the spine on the ornithopter performance. However, before examining the kinematics, the research team had to ensure that free flight in the test chamber could be achieved and that the ornithopter was supporting

its own weight and completely off the tether. Figure 5.4 (a) shows a flight data sample of the ornithopter's flight path with the four compliant joints inserted in its wings. The figure shows that the flight path (red) was well above the threshold (black) above which the ornithopter is no longer hanging on the tether. Thus free flight was indeed achieved. Also Figure 5.4 (b) shows the 3D markers location of the same wing configuration shown in Figure 5.4 (a) and therefore the wing kinematics of the ornithopter. The wing kinematics shown are for about 9 flapping cycles. From the Figure, it is clear that repeatable and consistent wing flaps were achieved. The standard deviation of the x, y, and z location of the markers was calculated to be 0.4 mm.



(a)

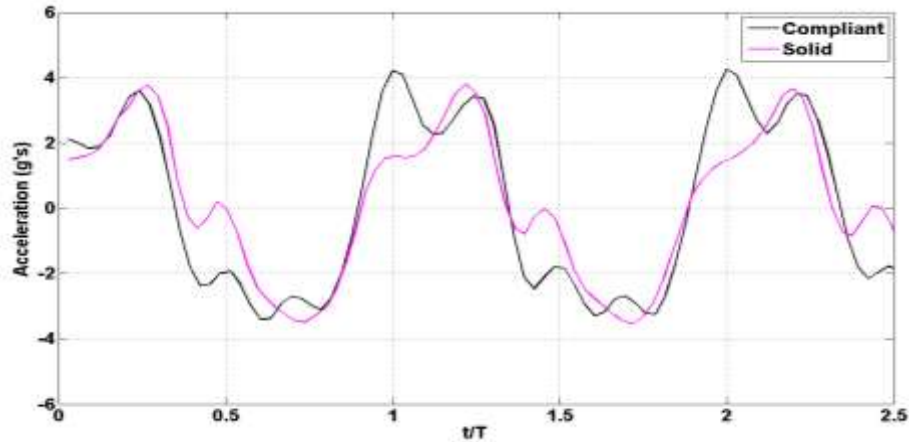


(b)

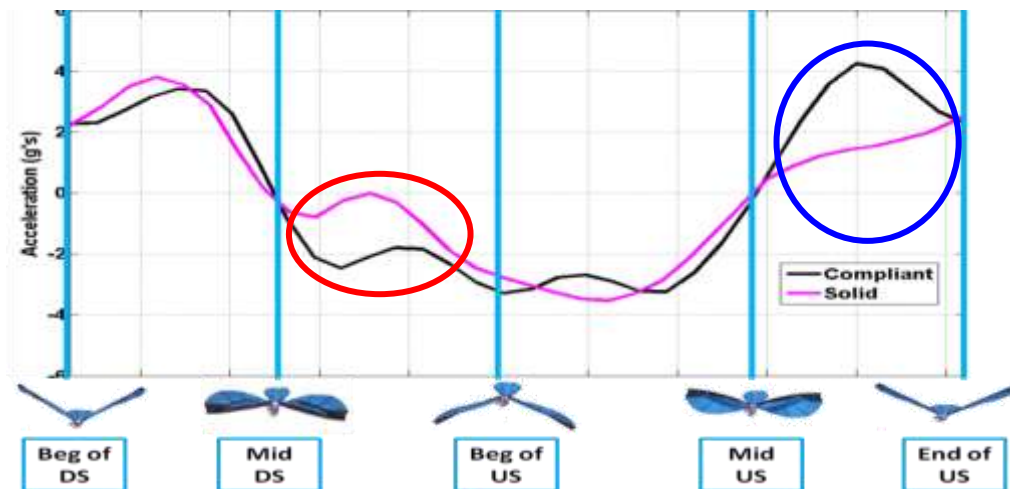
Figure 5.4 (a) Ornithopter fuselage flight path and proof of free flight (b) 3D markers position showing repeatable wing kinematics for 9 flapping wing cycles.

In order to study the effect of the presence of the compliant mechanism on the loads produced by the ornithopter, a rigid body model was fitted to the fuselage and the acceleration of the center of mass was calculated. Figure 5.5 shows the fuselage center of mass acceleration of the ornithopter with (black) and without (magenta) a four compliant joint compliant spine inserted in its wings. For the most part the acceleration curves were similar; however during the second half of the upstroke the ornithopter with the

compliant mechanism experienced an acceleration peak that was not present in the solid ornithopter during the second half of the upstroke where the compliant spine was most deflected (blue circle). On the other hand, during the second half of the downstroke, the ornithopter with the solid spar produced more acceleration than the ornithopter with the compliant spine (red circle). This acceleration reduction was due to the presence of the contact gaps in the compliant spine so that some undesirable deflections occurred during the downstroke. Preliminary data analysis results show that the ornithopter with the compliant spine reduced the overall negative center of mass acceleration during one flapping cycle by 22%. The negative acceleration reduction may translate into overall lift gains, which would confirm the bench test results mentioned in section 5.1.



(a)



(b)

Figure 5.5.(a) Fuselage center of mass vertical acceleration (g's) versus number of flapping cycles (t/T) for the ornithopter with (black) and without (magenta) a compliant spine inserted in its wings leading edge. (b) Fuselage center of mass vertical acceleration (g's) for the ornithopter with and without a compliant spine inserted in its wings leading edge for one flapping cycle.

6. Conclusions and future work

The overall goal of this work was to improve the steady level flight performance of ornithopters via passive wing morphing using a novel compliant spine. A multi-objective optimization was carried out and several designs resulting from this optimization were bench-top and free flight tested. The presence of a 1DOF compliant spine in the ornithopter wing was found to introduce an asymmetry between the upstroke and the downstroke. For any given flapping frequency or throttle setting, the ornithopter with the compliant spine consumed less electric power, produced more mean lift and did not incur any thrust penalties when compared to the ornithopter without the compliant spine. Thus the steady level flight performance was improved due to the presence of the compliant spine. Therefore compliant mechanisms proved to be not only feasible, but also beneficial for application to general air vehicle design.

A follow on project will begin in early 2013 focused on developing methods to design spatially-distributed 3DOF compliant elements, and to develop the associated models to predict the dynamic coupling between those elements. Validation and verification of the outcomes of the proposed research will be performed by applying the techniques developed to the current avian-scale ornithopter test platform in order to achieve full 3D passive shape change and to quantify the improvement in agility and maneuverability in addition to steady level flight.

7. References

- [1] Shyy, W., Berg, M. and Ljungqvist, D., 1999, "Flapping and Flexible Wings for Biological and Micro Air Vehicles," *Progress in Aerospace Sciences*, 35(5), 455-505.
- [2] Tobalske, B. W. and Dial, K. P., 1996, "Flight kinematics of black-billed magpies and pigeons over a wide range of speeds," *Journal of Experimental Biology*, 199(2), 263-280.
- [3] Tobalske, B. W., 2000, "Biomechanics and Physiology of Gait Selection in Flying Birds," *Physiological and Biochemical Zoology*, 73(6), 736-750.
- [4] Fenelon, M. A. A. and Furukawa, T., "Design of an active flapping wing mechanism and a micro aerial vehicle using a rotary actuator," *Mechanism and Machine Theory*, 45(2), 137-146.
- [5] McDonald, M. and Agrawal, S. K., 2010, "Design of a Bio-Inspired Spherical Four-Bar Mechanism for Flapping-Wing Micro Air-Vehicle Applications," *Journal of Mechanisms and Robotics*, 2, 6.
- [6] Cox, A., Monopoli, D., Goldfarb, M. and Garcia, E., 1999, "Development of piezoelectrically actuated micro-aerial vehicles", Boston, MA, USA, Society of Photo-Optical Instrumentation Engineers, 101-108.
- [7] Wissa, A., Tummala, Y., Hubbard Jr., J. E., and Frecker, M 2012 Passively Morphing Ornithopter Wings using a Novel Compliant Spine: Design and Testing," *Smart Materials and Structures* 21 094028.
- [8] Mueller, D., Gerdes, J. W., Gupta, S. K. , 2009, "Incorporation Of Passive Wing Folding In Flapping Wing Miniature Air Vehicles", *International Design Engineering Technical Conferences & Computers and Information in Engineering Conference*, San Diego, California.
- [9] Billingsley, D., Grauer, J., Hubbard, J., 2009, "Testing of a Passively Morphing Ornithopter Wing", *AIAA AUU* Seattle, Washington.
- [10] Brown, R. H. J., 1952, *The Flight of Birds: Wing Function in Relation to Flight Speed* Zoological Department, University of Cambridge.
- [11] Tummala, Y., Wissa, A., Frecker, M., Hubbard Jr., J. E., 2010, "Design of a Passively Morphing Ornithopter Wing Using a Novel Compliant Spine", *Proceedings of Smart Materials, Adaptive Structures and Intelligent Systems Conference*, Philadelphia, PA, United States.

- [12] Deb, K., 2001, *Multi-Objective Optimization Using Evolutionary Algorithms*, Chichester; New York, John Wiley & Sons.
- [13] Deb, K., Pratap, A., Agarwal, S. and Meyarivan, T., 2002, "A Fast and Elitist Multi-objective Genetic Algorithm: NSGA-II," *IEEE Transactions on Evolutionary Computation*, 6(2), 182-197.
- [14] Harmon, R., 2009, *Aerodynamic Modeling of Flapping Membrane Wing Using Motion Tracking Experiments*, Aerospace Engineering. College Park, University of Maryland. Master's Thesis
- [15] Wissa A, Tummala Y, Hubbard J E Jr and Frecker M., 2011 Testing of novel compliant spines for passive wing morphing Proc. Smart Materials, Adaptive Structures and Intelligent Systems Conf. (Scottsdale, AZ)